



heritage

IMPACT
FACTOR
1.9

CITESCORE
3.7

Article

Multi-Analytical Study of Lime-Based Mortars from the 16th-Century Venetian Fortress of Bergamo (Italy)

Renato Pelosato, Isabella Natali-Sora, Virna Maria Nannei and Giulio Mirabella Roberti

Special Issue

Non-Invasive Methods for Analysis and Diagnostic in the Field of Cultural Heritage

Edited by

Prof. Dr. Paola Fermo and Dr. Giuseppe Politi



<https://doi.org/10.3390/heritage8100400>

Article

Multi-Analytical Study of Lime-Based Mortars from the 16th-Century Venetian Fortress of Bergamo (Italy)

Renato Pelosato *, Isabella Natali-Sora *, Virna Maria Nannei and Giulio Mirabella Roberti 

Dipartimento di Ingegneria e Scienze Applicate, Università degli Studi di Bergamo, Viale Marconi n.5, 24044 Dalmine, BG, Italy; virnamaria.nannei@unibg.it (V.M.N.); giulio.mirabella@unibg.it (G.M.R.)

* Correspondence: renato.pelosato@unibg.it (R.P.); isabella.natali-sora@unibg.it (I.N.-S.)

Abstract

Mortars taken from the 16th century Venetian Fortress of Bergamo (Italy) were characterized (binder-concentrated fractions and aggregate fractions as well as bulk samples) with a multi-analytical approach using X-ray diffraction (XRD), inductively coupled plasma optical emission spectrophotometry (ICP-OES), optical microscopy (OM), differential scanning calorimetry (DSC) and thermogravimetric analysis (TG). The results showed the presence of calcite, hydrocalumite and hydrotalcite-type compounds, brucite, aragonite, plumbierite and a large fraction of amorphous phases (ranging between 14 and 27 wt%) in the binder. Quartz and carbonate-rich sands were used as aggregates. The mortar is a Mg-rich material containing 4–5 wt% brucite. No evidence of magnesite or hydromagnesite was found in any sample, although these phases are frequently detected in the binder of buildings from the Renaissance period that are located in Northern Italy. The large average amount (12–13 wt%) of reactive silicate, such as Mg-containing phyllosilicates that can react with lime, and the presence of carbonate-containing hydrocalumite and hydrotalcite indicate hydraulic interactions between lime and reactive silicate aggregates. The $\text{CO}_2/\text{H}_2\text{O}_{\text{bound}}$ ratio, evaluated from the weight loss referred to the finer fraction ($<63 \mu\text{m}$), ranges from 1.99 to 2.55, which suggests that the walls of Bergamo were constructed using lime-based mortar with hydraulic properties.



Academic Editors: Paola Fermo and Giuseppe Politi

Received: 8 August 2025

Revised: 16 September 2025

Accepted: 18 September 2025

Published: 23 September 2025

Citation: Pelosato, R.; Natali-Sora, I.; Nannei, V.M.; Mirabella Roberti, G. Multi-Analytical Study of Lime-Based Mortars from the 16th-Century Venetian Fortress of Bergamo (Italy). *Heritage* **2025**, *8*, 400. <https://doi.org/10.3390/heritage8100400>

Copyright: © 2025 by the authors. Licensee MDPI, Basel, Switzerland. This article is an open access article distributed under the terms and conditions of the Creative Commons Attribution (CC BY) license (<https://creativecommons.org/licenses/by/4.0/>).

Keywords: historic mortar; hydraulic mortar; brucite; hydrocalumite and hydrotalcite

1. Introduction

In fortified heritage conservation, most information and technical data refer to stone materials. However, the assessment of the state of conservation of fortified structures and, eventually, their restoration works also require knowledge of the composition of the historical mortar and the construction techniques adopted [1]. In particular, high-thickness walls are very often built as multi-leaf walls, where only external leaves are regularly arranged, but the internal leaves are made with rubble bonded by mortar. The binder is the main component of mortar; it ensures adhesion among all the components of the mortar, providing mechanical strength to the mixture by forming a hardened matrix that embeds the aggregates. The most common binders that have been used since the XIX century are Portland cement, lime, and gypsum. Historically, however, lime mortars, both in their hydraulic and non-hydraulic forms, were the most widely used mortars for centuries, although earth mortars were also employed, especially in vernacular architecture. Other mortar ingredients are fine aggregates (sand) and water, with possible additions of various components to tailor workability, setting time, or durability. Lime-based mortars

can be divided into two categories: air-hardening mortars and hydraulic mortars. The classification is based on the type of components and the mechanism that determines the hardening of the mortar. Specifically, air lime initially sets by drying and then slowly hardens in air by reacting with carbon dioxide (CO_2) and moisture in the air to form a carbonate (carbonatation). Hydraulic lime partly sets and hardens in response to chemical interaction with water, partly as a result of carbonatation. Its ability to harden in a wet environment can be attributed to the presence of certain compounds (calcium silicates and calcium aluminates) that react on contact with water to form hydrated hydraulic phases, which cause the mortar to harden.

Lime is obtained from limestone, which is a sedimentary rock consisting primarily of calcium carbonate (CaCO_3). It may contain impurities such as magnesium carbonate (MgCO_3) or dolomite ($\text{CaMg}(\text{CO}_3)_2$), clay minerals, iron oxides, silica (SiO_2), and feldspars, among others. During the high-temperature calcination of limestone (above $900\text{ }^\circ\text{C}$), the hydraulic components can form through the reaction of calcium oxide with compounds containing silicon and aluminum. The latter phases may already be present as impurities in the original limestone (e.g., marly limestone, which contains clay) or may be specifically added to the mix (e.g., pozzolana/cocciopesto).

For the analysis of ancient mortars, a multi-analytical approach is largely recommended in the literature [2], especially when assessing the hydraulicity of mortars. Many examples can be found in the literature; we will focus on the analysis of mortars from ancient sites in Italy. Most of the available literature of course concentrates on Roman materials, but a few examples of analyses of Middle Ages and Renaissance sites are also provided: Dilaria et al. [3] analyzed Roman mortars from three different sites in Italy—Aquileia (Northern Italy), Nora (Sardinia), and Pompeii (Naples)—and they used optical microscopy, X-Ray powder diffraction, SEM-EDS, and MAS-SS NMR to infer the hydraulicity of the mortars by identifying crystalline AFm-like structures like tobermorite or different forms of non-crystalline hydration products as calcium aluminate hydrates (C-A-H), calcium aluminate silicate hydrates (C-A-S-H), calcium silicate hydrates (C-S-H), and magnesium-rich materials such as magnesium silicate hydrate and magnesium aluminate silicate hydrate (M-S-H and M-A-S-H). In a detailed analysis of the waterproof coating of cisterns in the archeological site of Nora (Southern Sardinia, Italy) [4], a mix of petrographic, mineralogical, microstructural, and chemical analyses allowed Dilaria and coauthors to identify the specific treatments of the binders (like pozzolanic addition, comminution processes, etc.) that allowed the mortar to gain its hydraulic properties. C-S-H and AFm phases were accompanied in this case by anthropogenic magnesium silicate hydrate (M-S-H) gels. Artioli et al. [5] discuss in depth the role of LDHs (Layered Double Hydroxides) in the pozzolanic reactions in mortars spanning from Roman pozzolanic concrete to late Roman cocciopesto up to medieval earthen and earthen/pozzolanic mortars, highlighting that any Mg- and Al-containing material added to lime (as natural clay, fired pottery or others) leads to the formation of LDH-like phases (of which hydrotalcite is the most common) rather than portlandite in the hardened mortars. Bertolini et al. [6] investigated binders of mortars of San Lorenzo church in Milan, where Roman, Middle Ages, and Renaissance samples coexist. Using XRD, TG, and SEM techniques, it was found that if cocciopesto hydraulic mortars were used only in the Roman period, magnesium-rich lime binders containing silico-aluminates were instead common among mortars from all periods. Rizzi and coauthors [7] focused on a multi-analytical characterization of the mortars used for the construction of the fortified medieval settlement of Satrianum in Southern Italy. The rare earth element abundance was exploited to infer the provenance of materials used in the construction. The medieval castles of Châtel Argent and Quart (Aosta Valley, NW Italy) were the focus of the work by Milanese and coauthors [8]. They estimated the

hydraulic properties of the binders by calculating the hydration index (H.I.) based on the percentage composition in oxides ($\text{SiO}_2/\text{Al}_2\text{O}_3/\text{Fe}_2\text{O}_3/\text{MgO}/\text{CaO}$). They reported that magnesium-rich binders were used and showed a large span of hydraulic properties, from purely aerial binders in most of the samples to weakly hydraulic ones and up to properly hydraulic binders. The analysis was used to infer the origin of the materials and to suggest sources of restoration works.

The 12th–13th century Abbey of Santa Maria di Cerrate (Lecce, Apulia, South Italy), was investigated via multidisciplinary analyses to support conservators and art historians for its safeguard [9]; again, the investigations on mortars and aggregate composition allowed to identify the provenience of the materials used in the construction. In San Saturnino Basilica (Italy), an archeological mortar stratigraphy from Roman to Middle Ages is well preserved [10]. The physical–mechanical, mineralogical, petrographic, and thermal features suggested that Medieval materials were of a better quality than Roman ones, in terms of higher hydraulicity, mechanical performance, and a more appropriate particle-size distribution of aggregates. Recently, a mixed mineralogical–statistical approach has been proposed for historical mortars from Pompeii (Italy) [11–13] and Caesarea Maritima (Israel) [14] to analyze large datasets and facilitate the extraction of valuable information such as construction chronologies or technologies.

The main objective of this study was to evaluate mineralogical composition to determine the supply of raw materials and the constructive techniques of the historical mortars of the Venetian Fortress of Bergamo in the Lombard region of Italy. A multi-analytical approach was used to obtain coherent and reliable results. The approach comprised inductively coupled plasma optical emission spectrophotometry (ICP-OES), energy-dispersive spectroscopy (EDS), X-ray powder diffraction (XRPD), optical microscopy (OM), differential scanning calorimetry (DSC), and thermogravimetric analysis (TG).

2. Case Study: The Venetian Fortress of Bergamo

The Venetian fortress of Bergamo (Figure 1) was constructed by the Republic of Venice to defend the westernmost outpost of its territories. Bergamo was, in fact, situated on the border with the Ducato di Milano, near vital communication routes with Northern Europe [15]. Based on Governor Sforza Pallavicino's proposal to build a bastioned fortress capable of resisting firearms, work began in the summer of 1561. The initial plan was to allocate resources mainly to building the Fort of San Marco to the north and to using earthworks and parts of the medieval walls for the southern section, with some earth or stone bastions used at strategic points. By 1565, the defensive perimeter, which was just over 5 km long, comprised new stone walls in the northern section between Porta Sant'Alessandro and the San Lorenzo bastion, while in the southern part, the only new stone structure was the S. Grata platform. However, shortly after work commenced, it was decided that the entire circuit should be composed of new masonry structures. As a result, a project expected to take only a few months extended to a duration of 29 years. In 1590, the final bastion was completed, although further improvements continued in the following years [16].

The construction of the fortress significantly impacted the layout of the city, leading to the destruction of numerous buildings and changing the land's topography. However, from the 17th century onwards, attention to the fortress's military purpose waned, and the process of converting military sites for civilian use began. This was ultimately validated with the French domination starting in 1796 and the subsequent development of the promenade between Porta S. Agostino and Porta S. Giacomo. In 1812, the sale of land adjacent to the walls began. In 1825, the municipality acquired the areas on top of the ramparts from Porta S. Lorenzo to Porta S. Agostino and from Porta S. Giacomo to Porta S.

Alessandro. In 1829, work commenced on the road connecting Porta S. Giacomo and Porta S. Alessandro; however, the wall circuit remains almost entirely intact, except for a small section in the north-west, which was demolished in 1908 [17].



Figure 1. The Venetian Fortress of Bergamo. In red, the part of the walls object of the study.

The bastioned fortress with its 11 bulwarks and five platforms has, in recent decades, become a key aspect of the city's identity. This has led the municipality to advocate for its addition to the World Heritage List as part of the transnational site "The Venetian Works of Defence between 16th and 17th centuries: Stato da Terra—Western Stato da Mar" [18].

While inclusion in the UNESCO list acknowledged the significance of this fortification, it also underscored the challenge of maintaining such an extensive "stone landscape". To ensure proper and continuous upkeep of the walls, a collaborative project commenced in 2015. This initiative involved a partnership among the Municipality of Bergamo, the Università degli Studi di Bergamo, and Orobicambiente OdV. The initial phase of the project focused on surveying the wall circuit to evaluate its conservation status. Using aerial images, a 1:200 scale 3D model was created. This model facilitated the analysis of ongoing deterioration, which was primarily caused by invasive vegetation, and assisted in identifying critical zones, particularly in the north-western section known as the Forte di San Marco, which was situated between the San Lorenzo and Sant' Alessandro gates. As a result, a preliminary conservation plan for the entire complex was developed [19]. During the second phase of research, a thorough investigation was conducted into the bastions of San Pietro and Valverde, areas that were severely damaged by unchecked vegetation growth. These formed part of the so-called "Fort of San Marco," the north-western section of the fortress that was designed to accommodate the garrison and war materials, and as mentioned earlier, the first section to be constructed in stone. The findings from the diagnostic campaign informed the development of suitable strategies to reinforce the compromised sections of the wall, especially the upper parts of the eastern curtain wall and the northern spur of the Valverde bastion. These strategies were implemented in a pilot project, which will serve as a model for future work.

The diagnostic campaign, conducted through SABE and Orobicambiente, utilized a laser scanner and an aerial photogrammetric survey to create a 1:50 scale three-dimensional digital model of the two bastions [20]. This model facilitated discrete element structural analysis of the spur to assess its safety conditions [21]. Additionally, the model supported an archeological stratigraphic investigation to delineate the construction phases of this section of the walls. Lastly, the characterization of the construction materials included three vertical drillings into the foundation soil, six nearly horizontal drillings within the masonry thickness (Figure 2), and five geophysical sections executed on the foundation soil.



Figure 2. Horizontal drillings within the masonry thickness at the base of the walls (photo by Orobicambiente OdV, Beretta S.r.l., Besana in Brianza (MB), Italy).

The core samples show that the wall has an average thickness of around three meters. The rear face of the wall is fully buried, and in Valverde's case, the upper part is in line with the slope of the hill.

Archeological investigations on the east face of the Valverde bulwark struggled to distinguish between stratigraphic units due to several factors. The construction material was highly uniform in terms of lithotype, size, and workmanship, with the only exception being the limited reuse of Renaissance architectural material. The joints were often unstaggered, and large stones were present within sections of smaller size. Putlog holes were absent, and the masonry courses were variable in horizontality. These anomalies can be attributed to construction peculiarities, including the fact that the spurs were built first using large blocks of sandstone that fit together precisely, shaping the slope of the fortification's embankment. The blocks were crafted by skilled stonemasons whose marks can be seen on some of the ashlar. The curtain wall, on the other hand, consists of elements that are only roughly hewn by the masons, and are generally smaller in size, creating an irregular texture (Figure 3). Comparing the texture of the facing in this sector with the adjacent one towards Porta San Lorenzo, it appears that workers from diverse backgrounds and habits were assigned to different parts of the fortification's curtain wall simultaneously. The even more noticeable differences from the curtain walls on the southern side of the fortress suggest a substantial change in design approach implemented to complete the ring wall, which was driven by requests for a more refined appearance [22].



Figure 3. The east face of the Valverde bulwark. The spur displays large, precisely crafted sandstone blocks (photo by Orobicambiente OdV).

During geological investigations, nearly horizontal core samples were extracted from the masonry at the base of the walls. This enabled not only the verification of the wall's thickness but also the retrieval of many samples useful for assessing the consistency and composition of the masonry beyond its surface [23]. The core samples clearly reveal that the wall has a total thickness averaging 3 m; given that the wall stands approximately 10 m high, this thickness is substantial.

Mortars are crucial for the structural behavior of masonry, especially in thick walls where only the exterior is composed of cut stone. Additionally, the deterioration of mortar joints is a critical issue in masonry rehabilitation and significantly affects the overall aesthetic of the building. Given these considerations, conducting a more in-depth study of historical mortar is essential for developing an effective conservation plan for the fortress.

3. Materials and Methods

Figure 4 shows the locations from which the 9 core samples (named A, B, C, D, E, F, G, H, and I) were extracted. Nearly horizontal drillings through the masonry thickness were carried out at an approximate height of 1.50 m from the ground. The cores are from 2 to 4 m in length and contain parts of mortar, rocks and other filler materials used in the construction. A picture of the core extraction operations and of a 1.30 m long section of core F are reported in Figure 5, together with pictures of sections of mortars belonging to core F. Samples were taken from all 9 cores and divided into two sets for analysis (Table 1):

- (i) Spot samples: A total of 43 fragments of mortar were collected at different positions on the cores, corresponding to different depths in the wall. These specimens were ground and analyzed individually by X-Ray diffraction.
- (ii) Bulk samples: From 3 cores (namely B, D, and H) larger mortar samples of approximately 250 g were extracted. Each bulk sample was prepared by mixing several specimens extracted from different positions in the cores and grinding them together into one large powder sample in order to average the composition across the core. On the bulk samples XRD analysis, chemical analyses (ICP-OES or EDS), and TG-DSC measurements were performed.

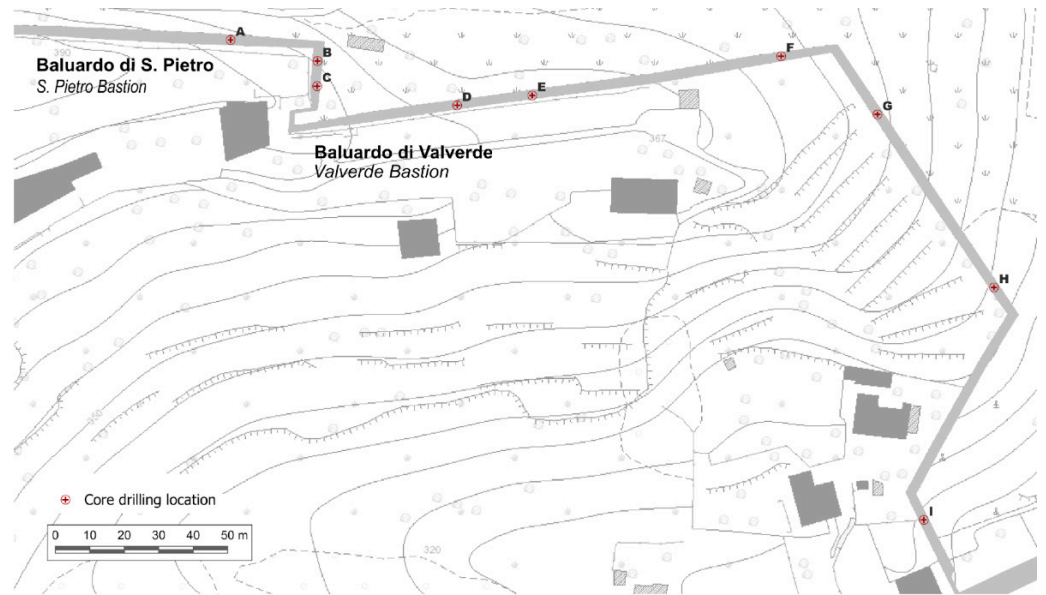


Figure 4. Plan of the Valverde and S. Pietro bastions with core sampling locations at the masonry base.

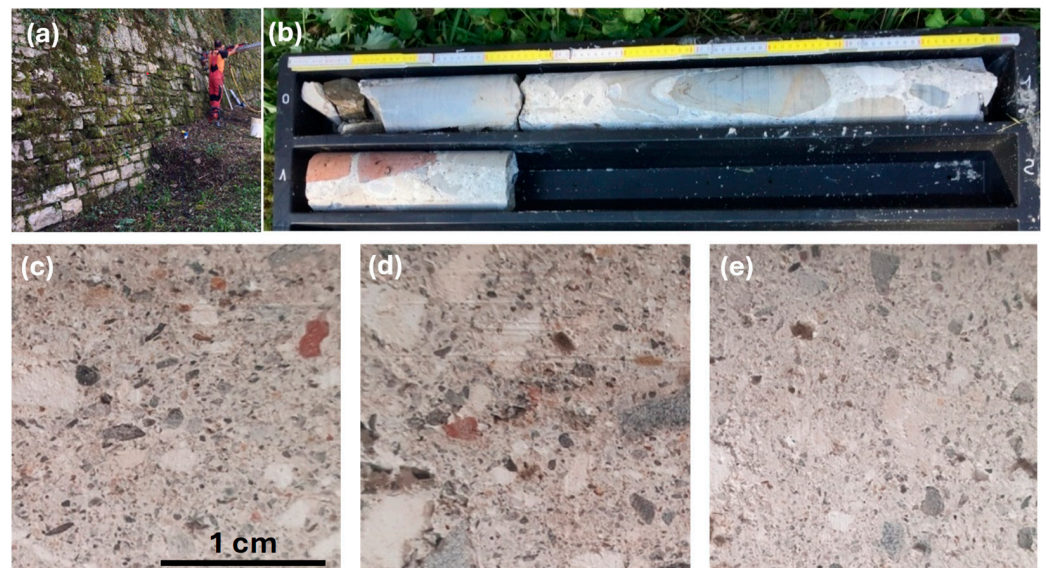


Figure 5. (a) Extraction of core F. (b) Segment of core F. (c–e) Pictures of sections of mortar taken from core F. The core can be divided into three parts: (i) from 0 to 0.40 m, Bergamo Flysch rock. (ii) From 0.40 to 1.00 m, well-consolidated portion consisting of fragments of lithotypes of various origins, with a predominance of Bergamo Flysch. Abundant presence of compact mortar. (iii) From 1.20 to 1.30 m, rock fragments of various origins bound together with mortar and the presence of anthropogenic clasts (red bricks).

Table 1. Distribution of the samples among the horizontal cores and the distance of the sampling locations from the external surface.

Core	Spot Samples (Number)	Depths (m)	Analytical Use	Bulk Samples (Number)	Analytical Use
A	4	0.30, 0.90, 1.20, 1.40	XRD	-	
B	5	0.65, 1.00, 1.20, 2.90, 3.65	XRD	1	XRD, TG-DSC, ICP-OES.
C	3	0.50, 0.95, 1.20	XRD	-	

Table 1. Cont.

Core	Spot Samples (Number)	Depths (m)	Analytical Use	Bulk Samples (Number)	Analytical Use
D	6	1.10, 1.70, 1.70, 2.55, 3.20, 3.20	XRD	1	XRD, TG-DSC, ICP-OES.
E	5	1.30, 1.50, 2.00, 2.50, 3.00	XRD	-	
F	5	0.20, 0.95, 0.95, 0.95, 1.30	XRD	-	
G	5	0.50, 1.00, 1.00, 1.50, 1.50	XRD	-	
H	5	0.40, 1.20, 1.50, 1.60, 1.60	XRD	1	XRD, TG-DSC, EDS.
I	5	0.50, 0.50, 1.05, 1.10, 1.50	XRD	-	
TOTAL	43			3	

3.1. Chemical and Mineralogical Characterization

Elemental analysis of mortars was performed by inductively coupled plasma optical emission spectrophotometry (ICP-OES) following UNI EN 16170:2016. Aqua regia was used as a digestion solution to extract elements from samples (UNI EN 16174:2012 method B). The main elements were (in order of abundance) Ca, Mg, Fe, Al, K, and Na (Table 2).

Table 2. Concentrations of the more abundant elements of binder fractions from cores B, D, and H (core H results are calculated by EDS measurements on powdered samples).

Species	Concentration (mg × kg ⁻¹)		
	Core B *	Core D *	Core H #
Ca	133,840	126,548	119,350
Mg	11,031	20,848	14,033
Fe	6180	6153	11,817
Al	6314	5549	7267
K	2887	1314	2850
Na	347	263	1833

* from ICP-OES; # from energy-dispersive spectroscopy (EDS).

X-ray diffraction (XRD) analysis was carried out on a powder diffractometer (Bruker D8 Advance, Bruker AXS Italia, Milano, Italy). The diffracted signal was collected using Lynxeye XE-T[®] solid-state detector. Measurements were performed in the $\theta/2\theta$ configuration using Cu K α radiation ($\lambda = 1.5418 \text{ \AA}$), with a voltage of 40 kV and a current of 40 mA. The scan range was 2–70° 2 θ with a step of 0.01° 2 θ and collection time of 19 per step. Patterns from 43 spot samples and 3 bulk samples of mortar (binder and aggregates) were collected. Millimeter-sized aggregates were separated from the materials before the measurements were performed. All samples were ground to smooth the surface of the powder before the measurements were obtained, in order to maximize the peak height and minimize scattering.

For the identification of the phases, the patterns were analyzed using DIFFRACPLUS EVA[®] version 5.1.0.5 software and the ICDD-PDF (International Centre for Diffraction Data—Powder Diffraction Files) database (version 2024). XRD was used to identify the mineralogical phases as well as to determine the semi-quantitative composition of the mortars by using the RIR (Reference Intensity Ratio) method as implemented within the EVA[®] software. The RIR is a general, instrument-independent constant for use in quantitative phase analysis by the X-ray powder diffraction internal standard method [24]. When the reference standard is corundum, RIR is known as I/I_c. These constants are

collected in the ICDD-PDF database. Phase analysis of diffraction patterns resulted in a large mineralogical dataset. Despite this feature, it was possible to quantify compositional differences among samples and subsequently group them based on similarities.

3.2. Petrographic Investigations

Petrographic investigations were carried out on samples collected from core drilling operations. Mortar samples were dried, cut and embedded in epoxy resin, polished and examined under transmitted and polarized light optical microscopy using a Zeiss Axioscope microscope (Carl Zeiss, Milano, Italy).

3.3. Thermogravimetric Measurements

Thermal analysis was carried out using a NETZSCH STA 300 simultaneous thermal analyzer (Netzsch Pompe & Sistemi Italia S.r.l., Verona, Italy). Approximately 25 mg of sample (a <63 μm fraction, separated by sieving) was placed in an alumina crucible and heated from 20 $^{\circ}\text{C}$ to 1150 $^{\circ}\text{C}$ at a heating rate of 5 $^{\circ}\text{C}/\text{min}$ under a flow of synthetic air (100 mL/min). The mass loss (TG) and its derivative (DTG), as well as the differential scanning calorimetry (DSC) signal, were recorded simultaneously.

4. Results and Discussion

From a macroscopic point of view, the samples showed good cohesion, and the color of the mortar was predominantly white or light gray (see Figure 5c–e). A significant number of small, pure white lumps could be identified, and were found to be spread evenly in all samples, as identified by visual inspection. Analyses of thin sections placed under an optical microscope showed that the aggregates were homogeneously distributed, and were identified as quartz, quartzite, limestone, and schist. An optical microphotograph of the mortar under crossed polars is reported in Figure 6.

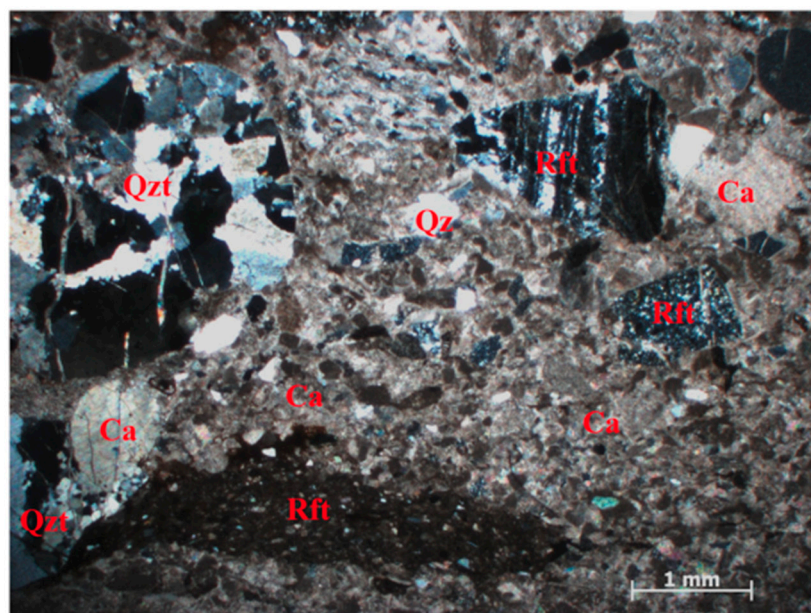


Figure 6. Microphotograph of mortar binder and aggregates under crossed polars (Ca = calcite binder, Qz = quartz, Qzt = quartzite, and Rft = fragments of other rocks (limestone and schists)).

XRD analysis was carried out to evaluate crystallinity and identify the phase composition in the mortar (the composition of all samples is reported in Table S1). XRD is a bulk technique. It can identify crystalline phases at a 1–2% mass fraction. The XRD phase quantification suggests good control of the mix design for the mortars.

The mineralogical characterization, reported in Figure 7 for bulk samples taken from cores B, D, and H, shows that the mortar mainly consists of 10 crystalline phases: calcite (CaCO_3); quartz (SiO_2); phyllosilicates such as muscovite ($\text{KAl}_2(\text{Si}_3\text{AlO}_{10})(\text{OH})_2$) and clinocllore ($(\text{Mg,Fe})_5\text{Al}(\text{Si}_3\text{Al})\text{O}_{10}(\text{OH})_8$); brucite $\text{Mg}(\text{OH})_2$; aragonite (CaCO_3); hydration products such as hydrocalumite-type ($\text{Ca}_4\text{Al}_2\text{O}_6(\text{CO}_3)_{0.5}(\text{OH}) \cdot 10.75\text{H}_2\text{O}$) and hydrotalcite-type ($\text{Mg}_6\text{Al}_2(\text{CO}_3)(\text{OH})_{16} \cdot 4\text{H}_2\text{O}$); inosilicates such as plombierite ($\text{Ca}_5\text{H}_2\text{Si}_6\text{O}_{18} \cdot 6\text{H}_2\text{O}$); and albite ($\text{NaAlSi}_3\text{O}_8$). Also, in a limited number of small samples of dolomite ($\text{CaMg}(\text{CO}_3)_2$) jennite ($\text{Ca}_9\text{Si}_6\text{O}_{18}(\text{OH})_6 \cdot 8\text{H}_2\text{O}$), vaterite (CaCO_3), and ettringite ($\text{Ca}_6\text{Al}_2(\text{SO}_4)_3(\text{OH})_{12} \cdot 24\text{H}_2\text{O}$) were spotted. The compounds quartz, muscovite, albite, and dolomite can be mainly attributed to the aggregate. Most of these minerals are consistent with the lithology of the Bergamo province [23], with the exception of dolomite, which was found as an aggregate in only a few samples. In addition to the crystalline compounds, the mortar contains a large fraction of amorphous phases (between 14 and 27 wt%; see Table S1). The amount of calcite quantified was partially attributed to the carbonation reaction in the hardening step of lime-binder $\text{Ca}(\text{OH})_2 + \text{CO}_2 \rightarrow \text{CaCO}_3 + \text{H}_2\text{O}$, and partially to the aggregate fraction, in agreement with petrographic observations. Moreover, in all cores, pure white and friable lumps were found, which contained 48–62 wt% of a mixture rich in $\text{Mg}(\text{OH})_2$ and CaCO_3 . As an example, in Figure 8 reports the XRD pattern obtained by analyzing a lump inside spot sample G-08 (see Table S1 for the complete semi-quantitative analysis). The XRD semi-quantitative analysis indicated that brucite is a component of the mortar (4–5 wt%), which agrees with the significant amount of Mg detected by the chemical analysis of the binder fraction of cores B, D, and H (Table 2).

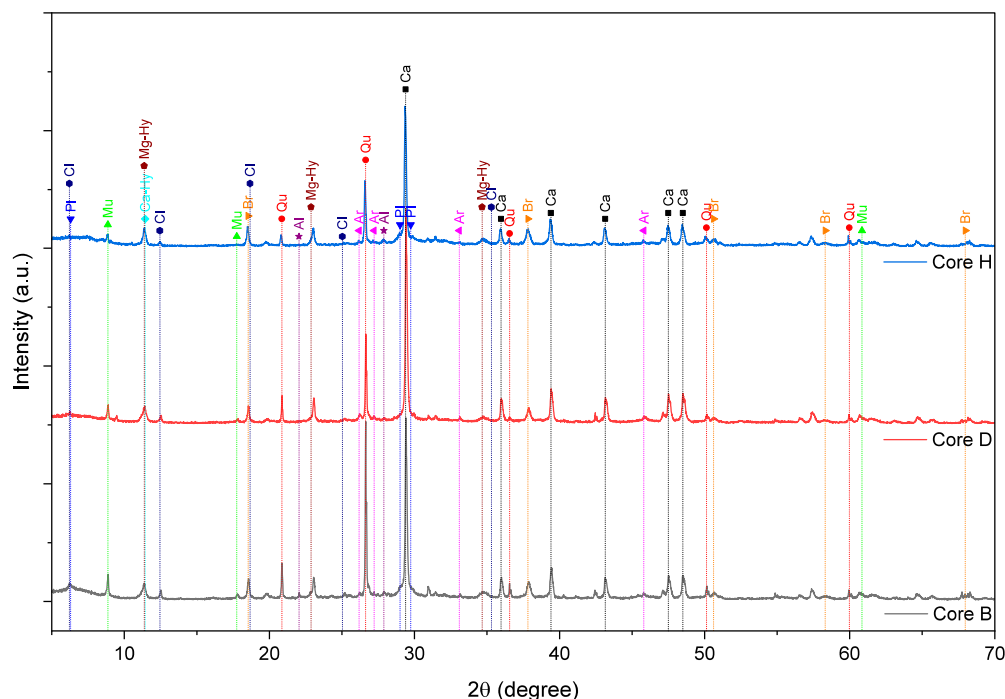


Figure 7. XRD patterns of bulk samples from cores B, D, and H. The main crystalline phases are Ca = calcite (CaCO_3), Ca-Hy = hydrocalumite-type ($\text{Ca}_4\text{Al}_2\text{O}_6(\text{CO}_3)_{0.5}(\text{OH}) \cdot 10.75\text{H}_2\text{O}$), Mg-Hy = hydrotalcite-type ($\text{Mg}_6\text{Al}_2(\text{CO}_3)(\text{OH})_{16} \cdot 4\text{H}_2\text{O}$), Br = brucite $\text{Mg}(\text{OH})_2$, Ar = aragonite (CaCO_3), Pl = plombierite ($\text{Ca}_5\text{H}_2\text{Si}_6\text{O}_{18} \cdot 6\text{H}_2\text{O}$), Qu = quartz (SiO_2), Mu = muscovite ($\text{KAl}_2(\text{Si}_3\text{Al})\text{O}_{10}(\text{OH})_2$), Cl = clinocllore ($(\text{Mg,Fe})_5\text{Al}(\text{Si}_3\text{Al})\text{O}_{10}(\text{OH})_8$), and Al = albite ($\text{NaAlSi}_3\text{O}_8$).

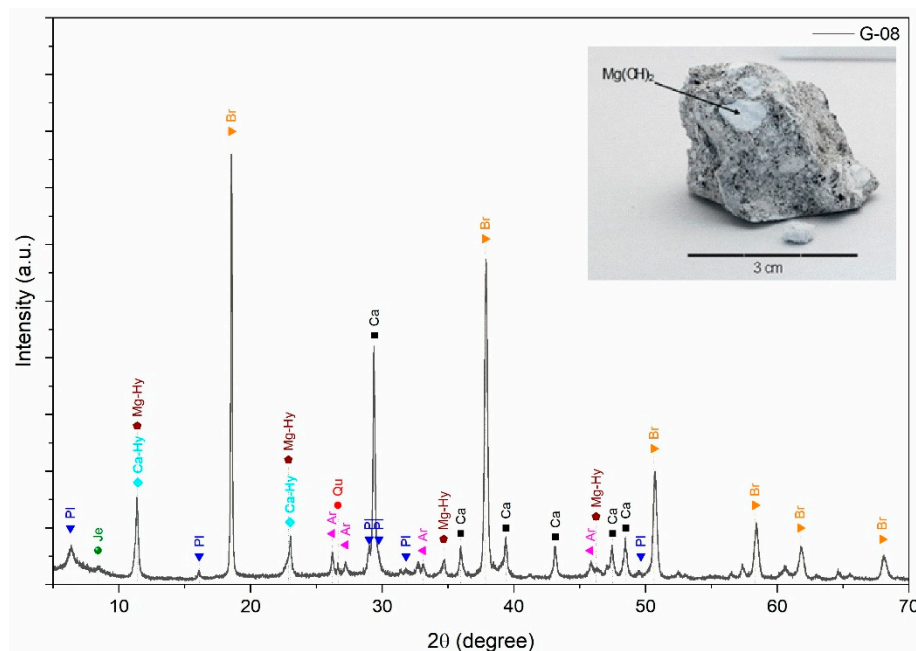


Figure 8. XRD pattern of the lump (spot sample G-08); in the inset picture of a specimen containing lumps of $\text{Mg}(\text{OH})_2$ and CaCO_3 . Br = brucite $\text{Mg}(\text{OH})_2$, Ca = calcite (CaCO_3), Ca-Hy = hydrocalumite-type ($\text{Ca}_4\text{Al}_2\text{O}_6(\text{CO}_3)_{0.5}(\text{OH}) \cdot 10.75\text{H}_2\text{O}$), Mg-Hy = hydrotalcite-type ($\text{Mg}_6\text{Al}_2(\text{CO}_3)(\text{OH})_{16} \cdot 4\text{H}_2\text{O}$), Ar = aragonite (CaCO_3), Pl = plombierite ($\text{Ca}_5\text{H}_2\text{Si}_6\text{O}_{18} \cdot 6\text{H}_2\text{O}$), Qu = quartz (SiO_2), Je = jennite ($\text{Ca}_9\text{Si}_6\text{O}_{18}(\text{OH})_6 \cdot (\text{H}_2\text{O})_8$).

In Table 2, elemental analyses of binder fractions of cores B, D (ICP-OES), and H (EDS) are reported. The elemental concentrations obtained show consistent trends, particularly with regard to the relative abundance of Ca, Mg, and Al. It must be noted that while ICP-OES gives precise quantitative data, EDS results are semi-quantitative, but allow a useful comparison of the amounts of the more abundant elements. As shown in Table 2, the average Mg/Ca mass to mass ratio is 0.08, 0.16, and 0.12 in cores B, D, and H, respectively, which is indicative of the presence of Mg-rich materials.

X-Ray diffraction analyses of both spot and bulk samples show no evidence of magnesite (MgCO_3) or hydromagnesite ($\text{Mg}_5(\text{CO}_3)_4(\text{OH})_2 \cdot 4\text{H}_2\text{O}$) compounds, although these phases are frequently detected in the binders of buildings from the Renaissance period that are located in Northern Italy [6,25].

The bedrock of Bergamo consists of a Cretaceous turbidite succession comprising sandstones, conglomerates, and marls. In particular, this substrate is composed of the so-called Bergamo Flysch [26–28], which is a gray/yellowish rock characterized by alternating layers of pelites and sandstones. In the Astino valley, less than 1500 m west of the fortress, in the territory of Bergamo town, a bank of marly limestone emerges, which is known to be a part of the Missaglia megabed [29]. It is possible that during the manufacturing of lime, a certain amount of limestone from local quarries standing on the Missaglia megabed was used, producing a moderately hydraulic lime. There is a report which states that the friars operated a kiln for lime burning in the Astino monastery in 1515 [30].

The occurrence of hydraulic reaction in the mortar is corroborated by three main features:

- (i) A large average amount of phyllosilicate clays, such as muscovite and clinocllore, was found in the mortar (12–13 wt% cumulative; see the XRD patterns in Figure 7 and semi-quantitative analyses in Table S1). Muscovite is an aluminum-rich clay ($\text{KAl}_2(\text{Si}_3\text{Al})\text{O}_{10}(\text{OH})_2$), while clinocllore contains a large amount of magnesium in its structure ($(\text{Mg,Fe})_5\text{Al}(\text{Si}_3\text{Al})\text{O}_{10}(\text{OH})_8$). According to Artioli et al. [31], and de-

pending on the temperature of the reaction, reactive aluminosilicate aggregates such as Mg-containing phyllosilicates can react with lime during the high-temperature calcination of limestone, yielding mixed Ca-, Mg-, Si-, and Al-containing reactive compounds, which may undergo hydration and carbonation reactions during the setting of the mortar. Arizzi and Parra-Fernández also suggest in Ref. [32] that the presence of carbonate-containing hydrocalumite ($\text{Ca}_4\text{Al}_2\text{O}_6(\text{CO}_3)_{0.5}(\text{OH})\cdot 10.75\text{H}_2\text{O}$) and hydrotalcite-type ($\text{Mg}_6\text{Al}_2(\text{CO}_3)(\text{OH})_{16}\cdot 4\text{H}_2\text{O}$) compounds in the hardened mortar is an indication that the above mechanism occurred between lime and reactive compounds (clays in this case). As illustrated above, those compounds were detected in all but a few samples extracted from the walls.

- (ii) Calcium silicate hydrate (C-S-H) in both amorphous and crystalline forms (jennite, tobermorite and plombierite) is the main type of hydration product formed in hydraulic mortars [2,33]. C-S-H (and, to a lesser extent, calcium aluminate hydrate, C-A-H) is formed by a complex process which primarily involves the hydration of calcium silicates (aluminates) present in hydraulic limes, and as an alternative to the reaction of silica and alumina potentially present in the mixture (originating from clays) with calcium hydroxide in wet conditions. With the exception of core F, these crystalline C-S-H phases (namely plombierite and jennite) were identified in 31 and 4 samples, respectively (see Table S1).
- (iii) A third clue comes from the presence of significant amounts of aragonite, which is a metastable polymorph of calcium carbonate, identified in some of the samples. It was detected in 48 samples in a 5wt% average amount (Table S1). Also, another metastable polymorph of calcium carbonate, vaterite, was found in a large concentration (22% in mass) in a lump belonging to core H (spot sample H-36b, Table S1). It is reported that the formation of metastable CaCO_3 polymorphs like aragonite and vaterite is indeed commonly favored by the presence of hydration products (C-S-H), and thus they are easily found when a hydraulic reaction has occurred [34–36].

The thermogravimetric profile (thermogram) is a graphical representation of the sample mass change vs. temperature or time. Commonly, a thermogram has multiple sections. (i) Below 150 °C, physically adsorbed water and trapped gases evolve. (ii) In the range of 150 °C ÷ 250 °C, mass loss occurs due to chemically adsorbed water and, if present, low-molecular-weight compounds such as additives. (iii) Above 250 °C, compounds begin to decompose. In the case of multicomponent mixtures, each component decomposes at a specific temperature. This also applies for reactions with intermediate steps. (iv) The material remaining above the end set temperature mainly comprises inorganic ashes.

The thermogram of the binder-sieved fraction (<63 µm) from core B, D, and H is reported in Figure 9. The plots reveal a multi-step mass loss pattern, with a total loss of around 30% at 1150 °C. The first derivative of the weight loss profile (DTG) identifies inflection points (peaks of the DTG). These features allow phenomena to be differentiated at overlapping temperatures. The initial weight loss below 150 °C is attributed to the removal of physisorbed water and, between 150 °C and 200 °C, possibly interlayer water in the layered double-hydroxide compounds like hydrotalcite (Mg/Al)- and hydrocalumite (Ca/Al)-type compounds [37]. A second, more pronounced mass loss occurs between 250 °C and 400 °C and is likely associated mainly with the de-hydroxylation of brucite ($\text{Mg}(\text{OH})_2$) [38] and hydrotalcite-like compounds [37]. This transformation is usually endothermic, which is confirmed by the corresponding DSC peaks in the same temperature range. A major mass loss step is observed between 600 °C and 850 °C, and corresponds to the decomposition of carbonate phases, primarily calcite (CaCO_3) and aragonite, releasing CO_2 . In addition, this process typically shows strong endothermic signals at 390 °C and a broad peak at 770 °C in the DSC curve.

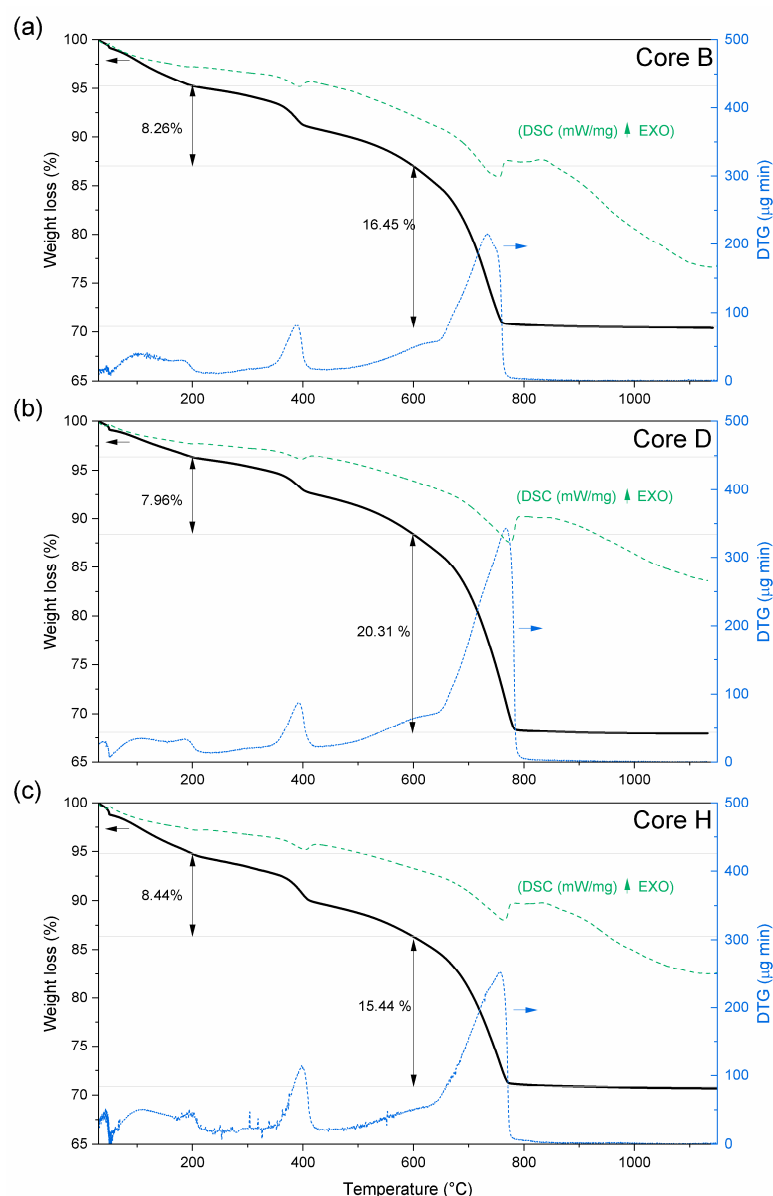


Figure 9. TG curve (black) and DTG curve (first derivative, in blue), of the binders' sieved fractions (<63 μm) heated to 1150 $^{\circ}\text{C}$ in air. The DSC curve is depicted in green (upward peaks denote exothermic processes). (a) Core B; (b) core D; (c) core H. The small black and blue arrows indicate the corresponding y-axis for the TG curve and the DTG curve, respectively.

One method of estimating hydraulicity relies on the amount of bound H_2O and CO_2 incorporated into the binder. These amounts can be easily extracted from thermogravimetric data. This method directly measures the amount of reaction products rather than their precursors, making it particularly suitable for characterizing the actual hydraulic behavior of the mortar after setting. Indeed, this index is often reported in this context, as demonstrated in references [39–41]. Thus, the ratio of the weight loss resulting from the decomposition of carbonates (>600 $^{\circ}\text{C}$) to that attributed to the chemically bound water of hydraulic compounds (200 ÷ 600 $^{\circ}\text{C}$), i.e., the $\text{CO}_2/\text{H}_2\text{O}_{\text{bound}}$ ratio, was calculated based on the weight loss associated with the finer fraction (<63 μm). The $\text{CO}_2/\text{H}_2\text{O}_{\text{bound}}$ ratio was 1.99, 2.55, and 1.83 for cores B, D, and H, respectively, which suggested that the mortar has a certain hydraulic character, according to the classification of Moropolou and coworkers [39,40]. This is only one of several measures used to evaluate mortar's hydraulicity. As reported in an in-depth review by Elsen and coworkers [42], a second

method refers to the hydraulicity index (*HI*) that dates back to 1818 and was defined as $HI = \frac{SiO_2 + Al_2O_3}{CaO}$. Later, it was expanded to include other oxides in $HI = \frac{SiO_2 + Al_2O_3 + Fe_2O_3}{CaO + MgO}$ based on the reactivity of the acidic (numerator) and alkaline (denominator) oxides. Still, it relies on a series of simplified assumptions about the reactivity of the available oxides in the binder (for instance, the assumption that all of the available SiO_2 reacts with CaO to form Ca_3SiO_5). The hydraulicity index, as formulated by Mariani [43], is still widely used in the context of historic binders; see, for example, Ref. [8]. According to this calculation, based on elemental analyses, the binder under study has an $HI = 0.20$ and an $HI = 0.18$ for mortars in core B and D, respectively, falling within the lower range of values for a medium hydraulic binder. It is worth noting that in the case of historic mortars, the starting oxide mixture is quantified based on XRF or ICP analyses of the hardened binder, which poses some uncertainties.

5. Conclusions

The historic mortars of the wall of Venetian Fortress of Bergamo show good cohesion and are predominantly white or light gray in color. Petrographic observations show that the aggregates are homogeneously distributed. Quartz and carbonate-rich sands were used as aggregates. The main elements of the binder fraction were Ca and Mg, with Mg/Ca ratio ranging from 0.08 to 0.16 (by ICP-OES and EDS analyses). Mineral phases present in the historic mortar were identified, leading to a preliminary characterization of binder and aggregate fractions. The main crystalline compounds were calcite; quartz; muscovite; hydrocalumite-type and hydrotalcite-type compounds; brucite; aragonite; plombierite; clinocllore; and albite. In all cores, pure white and friable lumps containing a mixture rich in brucite and calcite were found. The mortar also contains a large fraction of amorphous phases (between 14 and 27 wt%). The occurrence of hydraulic interactions in the mortar is corroborated by three features: (i) the large amount (12–13 wt% average) of phyllosilicate clays, muscovite, and clinocllore; (ii) the detection of jennite and plombierite in 4 and 31 samples, respectively; and (iii) the widespread presence of metastable polymorphs of calcium carbonate (containing more aragonite than vaterite). The thermogravimetric profile of the binder-sieved fraction (<63 μ m) provided important information regarding the hydraulic nature of the binder. The low CO_2/H_2O_{bound} ratio (in the range of 1.99 to 2.55) is in agreement with the presence of silicate and aluminate hydrated phases arising from hydraulic-type reactions. The moderate hydraulic character of the used lime suggests that it originated from quarries near the town, where a geological feature called “the Missaglia Megabed”, a continuous line of marly limestone, emerges at the surface. The selection and use of such materials was likely deliberate and informed by technical knowledge.

Supplementary Materials: The following supporting information can be downloaded at <https://www.mdpi.com/article/10.3390/heritage8100400/s1>, Table S1: Composition of samples in mortars obtained by XRD analysis. * indicates measurements performed on white lumps; ^ indicates the five measurements each on bulk samples of cores B, D, and H.

Author Contributions: Conceptualization, G.M.R.; Funding acquisition, G.M.R.; Investigation, R.P. and V.M.N.; Supervision, I.N.-S. and G.M.R.; Writing—original draft, I.N.-S. and V.M.N.; Writing—review and editing, R.P. and I.N.-S. All authors have read and agreed to the published version of the manuscript.

Funding: This research was funded by Fondazione Cariplo, grant n° 3068-2019, call 2019 “Arte e Cultura—Beni al sicuro”.

Acknowledgments: The authors gratefully acknowledge the help of Orobicambiente OdV and its volunteers for providing the aerial images and collaborating with us during the diagnostic campaign. The authors also thank Haroon Ahmad for his assistance with the TG-DSC measurements.

Conflicts of Interest: The authors declare no conflicts of interest. The funders had no role in the design of the study; in the collection, analyses, or interpretation of data; in the writing of the manuscript; or in the decision to publish the results.

References

1. Bokan Bosiljkov, V.; Padovnik, A.; Turk, T. (Eds.) *Conservation and Restoration of Historic Mortars and Masonry Structures: HMC 2022*; RILEM Bookseries; Springer Nature: Cham, Switzerland, 2023; Volume 42, ISBN 978-3-031-31471-1.
2. Arizzi, A.; Cultrone, G. Mortars and Plasters—How to Characterise Hydraulic Mortars. *Archaeol. Anthropol. Sci.* **2021**, *13*, 144. [[CrossRef](#)]
3. Dilaria, S.; Secco, M.; Rubinich, M.; Bonetto, J.; Miriello, D.; Barca, D.; Artioli, G. High-performing Mortar-based Materials from the Late Imperial Baths of Aquileia: An Outstanding Example of Roman Building Tradition in Northern Italy. *Geoarchaeology* **2022**, *37*, 637–657. [[CrossRef](#)]
4. Dilaria, S.; Secco, M.; Bonetto, J.; Ricci, G.; Artioli, G. Making Ancient Mortars Hydraulic. How to Parametrize Type and Crystallinity of Reaction Products in Different Recipes. In *Historic Mortars International Conference*; RILEM Bookseries; Springer: Berlin/Heidelberg, Germany, 2023; Volume 42, pp. 36–52.
5. Artioli, G.; Secco, M.; Addis, A.; Bellotto, M. 5. Role of Hydrotalcite-Type Layered Double Hydroxides in Delayed Pozzolan Reactions and Their Bearing on Mortar Dating. In *Cementitious Materials*; Pöllmann, H., Ed.; De Gruyter: Berlin, Germany, 2017; pp. 147–158, ISBN 978-3-11-047372-8.
6. Bertolini, L.; Carsana, M.; Gastaldi, M.; Lollini, F.; Redaelli, E. Binder Characterisation of Mortars Used at Different Ages in the San Lorenzo Church in Milan. *Mater. Charact.* **2013**, *80*, 9–20. [[CrossRef](#)]
7. Rizzo, G.; Buccione, R.; Curcio, R.; Gargiulo, B.; Sogliani, F. Multi-Analytical Characterization and Provenance Assessment on the Mortars of Satrianum (Italy). *Rend. Della Soc. Geol. Ital.* **2023**, *60*, 152–161. [[CrossRef](#)]
8. Milanese, E.; Storta, E.; Gambino, F.; Appolonia, L.; Borghi, A.; Glarey, A. Petrographic Characterization of Historic Mortar as a Tool in Archaeologic Study: Examples from Two Medieval Castles of Aosta Valley, Northwestern Italy. *J. Archaeol. Sci. Rep.* **2022**, *46*, 103719. [[CrossRef](#)]
9. Vasco, G.; Serra, A.; Buccolieri, G.; Manno, D.; Calcagnile, L.; Quarta, G.; Buccolieri, A. Mortar Characterization and Radiocarbon Dating as Support for the Restoration Work of the Abbey of Santa Maria Di Cerrate (Lecce, South Italy). *Heritage* **2022**, *5*, 4161–4173. [[CrossRef](#)]
10. Sitzia, F. The San Saturnino Basilica (Cagliari, Italy): An Up-Close Investigation about the Archaeological Stratigraphy of Mortars from the Roman to the Middle Ages. *Heritage* **2021**, *4*, 1836–1853. [[CrossRef](#)]
11. Secco, M.; Previato, C.; Addis, A.; Zago, G.; Kamsteeg, A.; Dilaria, S.; Canovaro, C.; Artioli, G.; Bonetto, J. Mineralogical Clustering of the Structural Mortars from the Sarno Baths, Pompeii: A Tool to Interpret Construction Techniques and Relative Chronologies. *J. Cult. Herit.* **2019**, *40*, 265–273. [[CrossRef](#)]
12. Dilaria, S.; Previato, C.; Secco, M.; Busana, M.S.; Bonetto, J.; Cappellato, J.; Ricci, G.; Artioli, G.; Tan, P. Phasing the History of Ancient Buildings through PCA on Mortars' Mineralogical Profiles: The Example of the Sarno Baths (Pompeii). *Archaeometry* **2022**, *64*, 866–882. [[CrossRef](#)]
13. Piovesan, R.; Dalconi, M.C.; Maritan, L.; Mazzoli, C. X-Ray Powder Diffraction Clustering and Quantitative Phase Analysis on Historic Mortars. *Eur. J. Mineral.* **2013**, *25*, 165–175. [[CrossRef](#)]
14. Secco, M.; Asscher, Y.; Ricci, G.; Tamburini, S.; Preto, N.; Sharvit, J.; Artioli, G. Cmentation Processes of Roman Pozzolan Binders from Caesarea Maritima (Israel). *Constr. Build. Mater.* **2022**, *355*, 129128. [[CrossRef](#)]
15. Fumagalli, A. Fortificazioni Venete a Bergamo. In *Le Mura di Bergamo*; Azienda Autonoma di Turismo: Bergamo, Italy, 1977; pp. 3–30.
16. Foppolo, V. La Costruzione Delle Mura Venete. In *Le Mura di Bergamo*; Azienda Autonoma di Turismo: Bergamo, Italy, 1977; pp. 31–62.
17. Capellini, P. Le Mura Dopo Il Dominio Veneto. In *Le Mura di Bergamo*; Azienda Autonoma di Turismo: Bergamo, Italy, 1977; pp. 325–348.
18. UNESCO. *World Heritage Committee Nominations to the World Heritage List 2017*; UNESCO: Paris, France, 2017.
19. Mirabella Roberti, G.; Nannei, V.M.; Azzola, P.; Cardaci, A. Preserving the Venetian Fortress of Bergamo: Quick Photogrammetric Survey for Conservation Planning. *Int. Arch. Photogramm. Remote Sens. Spat. Inf. Sci.* **2019**, *XLII-2/W11*, 873–879. [[CrossRef](#)]
20. Nannei, V.M.; Azzola, P.; Mirabella Roberti, G. From Survey to Analysis of the Damage Mechanisms in Stone Walls: Diagnostic Investigations on a Bastion of the Venetian Fortress in Bergamo. In *Proceedings of the 9th Rehabend Congress*, Granada, Spain, 13–16 September 2022; pp. 971–980.
21. Paris, V.; Gobbin, F.; Nannei, V.M.; Resmini, M.; Mirabella Roberti, G. Distinct Element Method Analyses for Damage Assessment: The Northern Spur of Valverde Bulwark in the Venetian Fortress of Bergamo. *Int. J. Archit. Herit.* **2025**, *19*, 687–701. [[CrossRef](#)]

22. Mirabella Roberti, G.; Gallina, D.; Nannei, V.M. La Costruzione Delle Mura Di Bergamo: Indagini Conoscitive Su Tecniche e Materiali. In *Oltre lo Sguardo. Beyond the Gaze. La Città Stratificata. The Layered City; Insights*; AISU International: Torino, Italy, 2025; Volume 3.
23. Marsetti, D. Indagine Geognostica Geologica. In *Il baluardo di Valverde: Una Ferita da Ricucire Nella Fortezza Veneziana di Bergamo*; Comune di Bergamo: Bergamo, Italy, 2020; p. 176.
24. Hubbard, C.R.; Snyder, R.L. RIR—Measurement and Use in Quantitative XRD. *Powder Diffr.* **1988**, *3*, 74–77. [[CrossRef](#)]
25. Bruni, S.; Cariati, F.; Fermo, P.; Pozzi, A.; Toniolo, L. Characterization of Ancient Magnesian Mortars Coming from Northern Italy. *Thermochim. Acta* **1998**, *321*, 161–165. [[CrossRef](#)]
26. Bini, A.; Bersezio, R.; Tucci, G.; Scardia, G.; Rigamonti, I.; Rossi, R.; Ferliga, C.; Carnati, S.; Kovacs, M.; Cislighi, L.; et al. Carta Geologica d'Italia alla scala 1:50000 Foglio 098: Bergamo. ISPRA, CARG 2012, Italy. Available online: https://www.isprambiente.gov.it/Media/carg/98_BERGAMO/Foglio.html (accessed on 9 July 2025).
27. Jadoul, F.; Forcella, F.; Bini, A.; Ferliga, C. *Carta Geologica Della Provincia Di Bergamo*; Provincia di Bergamo: Bergamo, Italy, 2000.
28. Bini, A.; Bersezio, R.; Tucci, G.; Scardia, G.; Rigamonti, I.; Rossi, R.; Ferliga, C.; Carnati, S.; Kovacs, M.; Cislighi, L.; et al. Carta Geologica d'Italia alla scala 1:50000 Foglio 097: Vimercate. ISPRA, CARG 2014, Italy. Available online: https://www.isprambiente.gov.it/Media/carg/97_VIMERCATE/Foglio.html (accessed on 9 July 2025).
29. Bernoulli, D.; Bichsel, M.; Bolli, H.M.; Haring, M.O.; Hochuli, P.A.; Kleboth, P. The Missaglia Megabed, a Catastrophic Deposit in the Upper Cretaceous Bergamo Flysch, Northern Italy. *Eclogae Geol. Helv.* **1981**, *74/2*, 421–442. [[CrossRef](#)]
30. Glanzer, M. La miniera di Astino, Bergamo, Italy, 2006. Available online: https://www.nottole.it/pubblicazioni/Nottografia_miniera_di_Astino.pdf (accessed on 9 September 2025).
31. Artioli, G.; Secco, M.; Addis, A. The Vitruvian Legacy: Mortars and Binders before and after the Roman World. In *The Contribution of Mineralogy to Cultural Heritage, EMU Notes in Mineralogy*; Mineralogical Society of Great Britain and Ireland: Twickenham, UK, 2019; Volume 20, Chapter 4, pp. 151–202. [[CrossRef](#)]
32. Arizzi, A.; Parra-Fernández, C. A Comprehensive Review of the Manufacturing Process and Properties of Natural Hydraulic Limes. *Mater. Struct. Constr.* **2025**, *58*, 152. [[CrossRef](#)]
33. Bonaccorsi, E.; Merlino, S.; Kampf, A.R. The Crystal Structure of Tobermorite 14 Å (Plombierite), a C-S-H Phase. *J. Am. Ceram. Soc.* **2005**, *88*, 505–512. [[CrossRef](#)]
34. Ricci, G.; Secco, M.; Marzaioli, F.; Terrasi, F.; Passariello, I.; Addis, A.; Lampugnani, P.; Artioli, G. The Cannero Castle (Italy): Development of Radiocarbon Dating Methodologies in the Framework of the Layered Double Hydroxide Mortars. *Radiocarbon* **2020**, *62*, 617–631. [[CrossRef](#)]
35. Shivakumar, M.; Selvaraj, T. Characterization Study on the Influence of Limestone and Shell Lime as a Fine Aggregate Substitute: A Traditional Approach on Lime Plaster Restoration. *Mater. Today Proc.* **2021**, *45*, 6519–6526. [[CrossRef](#)]
36. Jackson, M.D.; Mulcahy, S.R.; Chen, H.; Li, Y.; Li, Q.; Cappelletti, P.; Wenk, H.-R. Phillipsite and Al-Tobermorite Mineral Cements Produced through Low-Temperature Water-Rock Reactions in Roman Marine Concrete. *Am. Mineral.* **2017**, *102*, 1435–1450. [[CrossRef](#)]
37. Mokhtar, M.; Inayat, A.; Ofili, J.; Schwieger, W. Thermal Decomposition, Gas Phase Hydration and Liquid Phase Reconstruction in the System Mg/Al Hydrotalcite/Mixed Oxide: A Comparative Study. *Appl. Clay Sci.* **2010**, *50*, 176–181. [[CrossRef](#)]
38. Turner, R.C.; Hoffman, I.; Chen, D. Thermogravimetry of the Dehydration of Mg(OH)₂. *Can. J. Chem.* **1963**, *41*, 243–251. [[CrossRef](#)]
39. Moropoulou, A.; Bakolas, A.; Anagnostopoulou, S. Composite Materials in Ancient Structures. *Cem. Concr. Compos.* **2005**, *27*, 295–300. [[CrossRef](#)]
40. Bakolas, A.; Biscontin, G.; Moropoulou, A.; Zendri, E. Characterization of Structural Byzantine Mortars by Thermogravimetric Analysis. *Thermochim. Acta* **1998**, *321*, 151–160. [[CrossRef](#)]
41. Gleize, P.J.P.; Motta, E.V.; Silva, D.A.; Roman, H.R. Characterization of Historical Mortars from Santa Catarina (Brazil). *Cem. Concr. Compos.* **2009**, *31*, 342–346. [[CrossRef](#)]
42. Elsen, J.; Van Balen, K.; Mertens, G. Hydraulicity in Historic Lime Mortars: A Review. In *Historic Mortars*; Válek, J., Hughes, J.J., Groot, C.J.W.P., Eds.; RILEM Bookseries; Springer: Dordrecht, The Netherlands, 2012; Volume 7, pp. 125–139, ISBN 978-94-007-4634-3.
43. Mariani, E. *Leganti: Aerei e Idraulici*; Casa Editrice Ambrosiana: Milan, Italy, 1976.

Disclaimer/Publisher's Note: The statements, opinions and data contained in all publications are solely those of the individual author(s) and contributor(s) and not of MDPI and/or the editor(s). MDPI and/or the editor(s) disclaim responsibility for any injury to people or property resulting from any ideas, methods, instructions or products referred to in the content.